A global model: Empirical orthogonal function analysis of total electron content 1999–2009 data

Ercha A,[1,2] Donghe Zhang,[1,3] Aaron J. Ridley,[2] Zuo Xiao,[1,3] and Yongqiang Hao[1]

Received 7 October 2011; revised 6 January 2012; accepted 1 February 2012; published 27 March 2012.

[1] A global ionospheric total electron content (TEC) model based on the empirical orthogonal function (EOF) analysis method is constructed using the global ionosphere maps provided by Jet Propulsion Laboratory during the years 1999–2009. The importance of different types of variation to the overall TEC variability as well as the influence of solar radiation and geomagnetic activity toward TEC can be well represented by the characteristics of EOF base functions E_k and associated coefficients P_k. The quick convergence of EOF decomposition makes it possible to use the first four orders of the EOF series to represent 99.04% of the overall variance of the original data set. E_1 represents the essential feature of global spatial and diurnal variation of the TEC. E_2 contains a hemispherically asymmetric pattern manifesting the summer-to-winter annual variation. E_3 and E_4 can well reflect the equatorial anomaly phenomenon. P_1 contains an obvious solar cycle variation pattern as well as annual and semiannual variation components. P_2 mainly includes an annual fluctuation component. P_3 has a strong annual variation and a weak seasonal variation pattern. P_4 has both evident annual and semiannual oscillation components. The Fourier series as a combination of trigonometric and linear functions are used to represent the solar cycle, annual, and semiannual variation of the coefficients. Therefore the global TEC model is established through incorporating the modeled EOF series. The accuracy and quality of the model have been validated through the model-data comparison, which indicates that the model can reflect the majority of the variations and the feature of temporal-spatial distribution of the global ionospheric TEC.

Citation: A, E., D. Zhang, A. J. Ridley, Z. Xiao, and Y. Hao (2012), A global model: Empirical orthogonal function analysis of total electron content 1999–2009 data, *J. Geophys. Res.*, *117*, A03328, doi:10.1029/2011JA017238.

1. Introduction

[2] Ionospheric variability is influenced by a number of factors which can be generally divided as solar ionizing radiation, geomagnetic activity, and meteorological influences [*Forbes et al.*, 2000; *Rishbeth and Mendillo*, 2001]. Ionospheric models have been playing an indispensable role in attributing different types of variations in the ionosphere as a function of above parameters and specifying the ionospheric environment as practically as possible. Ionospheric empirical models, which are mainly built on statistical analysis of extended data sets, utilize appropriate theory-based functions to manifest the intrinsic variations in the ionospheric parameters [*Bilitza*, 2002]. Empirical models typically represent the gross features in the ionosphere quite well, but are limited to the way the model was built, the data that was used to construct it, and the conditions that were occurring while the data was taken. First principle models, on the other hand, tend to not reproduce the data as well as empirical models, but can be run for a wider set of conditions. Further thought experiments can be run with first principle models to test theories. Therefore, it is clear that there remains a need for both types of models.

[3] The ionospheric total electron content (TEC) is one of the particularly important descriptive physical quantities of the ionosphere. TEC has been extensively investigated and modeled not only for the scientific research of ionosphere but also for applications such as satellite navigation, error correction to operational systems, determining the scintillation of radio wave, and satellite altimetry.

[4] The distribution of electron densities on which the construction process of a TEC empirical model is based can be acquired via at least two different ways. One is from existing empirical models such as the International Reference Ionosphere (IRI) model [*Bilitza*, 1990, 2001], which describes the profile of electron density and is driven by geographic and geomagnetic location, $F_{10.7}$, and geomagnetic activity level. A second method would be utilizing different TEC measurements at single or regional sites. Most early empirical TEC models were implemented based on three fundamental types of techniques for measuring the ionospheric TEC: Faraday rotation, Differential Doppler, and Group Delay methods. Some studies used the simultaneous Faraday

[1]Institute of Space Physics and Applied Technology, Peking University, Beijing, China.
[2]Department of Atmospheric, Oceanic, and Space Sciences, University of Michigan, Ann Arbor, Michigan, USA.
[3]State Key Laboratory of Space Weather, Chinese Academy of Sciences, Beijing, China.

0148-0227/12/2011JA017238

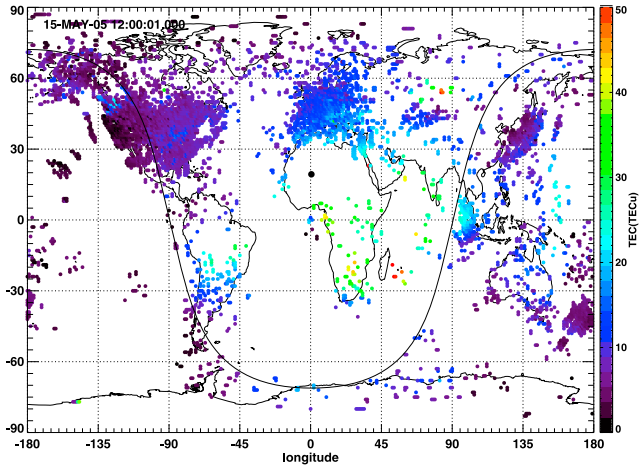

Figure 1. A sample plot of the global distribution of the total electron content (TEC). The terminator and the subsolar point are also marked.

rotation measurement of polarized signals to build the empirical models [e.g., *Poulter and Hargreaves*, 1981; *Gulyaeva*, 1999; *Unnikrishnan et al.*, 2002]. The European COST Actions 238 [*Bradley*, 1999] and Actions 251 [*Hanbaba*, 1999] constructed the regional TEC empirical models from Differential Doppler observations on the signals of the Navy Navigation Satellites Systems (NNSS). Recently, the GPS measurements obtained from the global and regional networks of International GNSS Service (IGS) ground receivers have been widely used to derive the TEC data over large geographic areas with high temporal and spatial resolution [*Mannucci et al.*, 1998; *Hernández-Pajares et al.*, 1999; *Zhang and Xiao*, 2003; *Mendillo*, 2006]. The GPS technique has great advantages in specifying the patterns of TEC morphology as well as producing real-time global ionosphere maps (GIMs) and regional ionosphere maps (RIMs) of TEC distribution [e.g., *Wilson et al.*, 1995; *Iijima et al.*, 1999; *Ping et al.*, 2002; *Orús et al.*, 2005; *Stolle et al.*, 2005; *Fuller-Rowell et al.*, 2006; *Sayin et al.*, 2008]. Therefore, a great number of new TEC empirical models based on GIMs/RIMs have been well developed. For example, *Habarulema et al.* [2010, 2011] built regional GPS-based TEC models over Southern Africa by using a neural network analysis method. *Bouya et al.* [2010] used Spherical Cap Harmonic Analysis (SCHA) to construct a regional ionospheric TEC model over Australia. *Mao et al.* [2008] proposed a climatological model of TEC over China using 9 years of GPS data utilizing empirical orthogonal function (EOF) analyses. *Wan et al.* [2008a] developed a global ionospheric TEC model using a statistical Eigen mode analysis method. In this paper, we will present a global TEC model that is constructed utilizing EOF decomposition of long-term TEC data from global ionosphere maps and regression analysis to fit the associated EOF coefficients. The primary purpose is to describe a compact means of reproducing the TEC GIMs provided by Jet Propulsion Laboratory (JPL). It is also expected to use this model to characterize the variability within the global TEC and identify the associated drivers of that variability. Moreover, we aim to make this model applicable under geomagnetic disturbance conditions to verify the reliability in capturing the dynamics of TEC in different conditions.

[5] In section 2, we will present a brief description of the TEC data used for the current study. The implementation of the EOF analysis to the global TEC data is then described in section 3. The validity and accuracy of the model are verified by a presentation of data-model comparisons in section 4, and the summary and conclusions are presented in section 5.

2. TEC Data Set

[6] The ionospheric TEC is derived by mapping the slant path delay of the signal from dual frequency L band (1.545 GHz and 1.226 GHz) observed by the global networks of IGS ground receivers [*Ge et al.*, 2004; *Dow et al.*, 2009]. Presently IGS manages a network of 436 stations and 371 active stations as of November 2011, which increased by more than 300 stations within one solar cycle. IGS provides the highest precision of GPS satellite orbits, and precise positions (5 mm) for 350 worldwide reference stations. Thus 6–8 simultaneous TEC measurements can be provided by each of the receivers covering the range of 1000 km [*Wan et al.*, 2008b]. Therefore the GIMs can be constructed with much higher resolution with respect to the increasing of the data points. Figure 1 displays a sample of global distribution of TEC. Usually the single ionospheric layer assumption is considered to convert the slant path TEC to vertical TEC (VTEC) with a mapping function. Currently, five analysis centers routinely provide GIMs of TEC using the ever-growing global network of dual frequency GPS receivers. These are the Center for Orbit Determination of Europe (CODE) [*Schaer*, 1999], JPL [*Ho et al.*, 1996], European Space Agency (ESA) [*Feltens and Schaer*, 1998; *Feltens*, 2007], Polytechnical University of Catalonia (UPC) [*Hernández-Pajares et al.*, 1997], and the Energy Mines and Resources Canada (EMR) [*Gao et al.*, 1994]. All the above products have a temporal resolution of 2 hours and spatial resolution of 2.5° (latitude) × 5° (longitude) with errors of several TEC Units (TECU, 1 TECU = 10^{16} el/m^2) [*Hernández-Pajares et al.*, 2009]. For the current study, we chose the global VTEC data from 1 January 1999 to 31 December 2009 provided by the JPL GIMs to establish the empirical model. For more details on the data retrieval, readers may refer to *Mannucci et al.* [1998].

3. Modeling Technique

3.1. Description of EOF Analysis Method

[7] The EOF analysis method, also known as Natural Orthogonal Component (NOC) algorithm or principal component analysis (PCA), was originally invented by *Pearson* [1901]. The physical essence of EOF theory is to reduce the dimensionality of a dataset consisting of multiple intercorrelated variables, while preserving the majority of the variation influenced by some independent processes as much as possible [*Jolliffe*, 2002]. This is done by using an orthogonal transformation to decompose the original data set into a set of uncorrelated and ordered base functions as well as associated coefficients. The orthogonal base functions are not predetermined artificially, but are derived from the original data set through decomposition processes. Moreover, each succeeding base function contains the variance present

Table 1. Summary of the Variances Through TEC Decomposition for the First Six Empirical Orthogonal Function (EOF) Series

EOF Series	Variances (%)	Cumulative Variances (%)
$E_1 \times P_1$	97.51	97.51
$E_2 \times P_2$	0.83	98.34
$E_3 \times P_3$	0.42	98.76
$E_4 \times P_4$	0.28	99.04
$E_5 \times P_5$	0.17	99.21
$E_6 \times P_6$	0.11	99.32

in the original variables as much as possible, which makes the EOF series converge rapidly. Therefore, it is possible to use only a few EOF base functions to describe the internal characteristic of the data, while the majority of the variance in data can be best represented. The advantages of the EOF analysis method have made it one of the preferred methods in the meteorological field to analyze the dominant components of temporal and spatial variations [*Lorenz*, 1956]. The EOF analysis method has also been used for empirical modeling of ionospheric and thermospheric variability [e.g., *Dvinskikh*, 1988; *Singer and Dvinskikh*, 1991; *Daniell et al.*, 1995; *Matsuo et al.*, 2002, 2005; *Marsh et al.*, 2004; *Zhao et al.*, 2005; *Zapfe et al.*, 2006; *Liu et al.*, 2008; *Mao et al.*, 2008; *Zhang et al.*, 2009, 2010; *Matsuo and Forbes*, 2010; *A et al.*, 2011; *Wan et al.*, 2012]. From the mathematical perspective, the orthogonal base functions, also called EOFs, are discrete functions of discrete variables. They are the eigenvectors of the covariance matrix formed from the original data matrix. For more details on the mathematical descriptions of the EOF analysis method, readers may refer to *Dvinskikh* [1988], *Storch and Zwiers* [1999], and *Xu and Kamide* [2004].

3.2. TEC Data Decomposition and Model Construction

[8] The original global TEC data were arrayed in terms of the coordinate system of geographical latitude and longitude. It is expected that the photoionization is the primary mechanism in producing ionospheric plasma. The dynamics of photoionization is basically influenced by the fact that the electrons are constrained to the magnetic field lines. The extent of photoionization is strongly dependent on local time [*Mannucci et al.*, 1998]. Hence the ionospheric variability and the features of ionospheric electrons are strongly *dependent* on the local time, geomagnetic latitude, solar ionizing radiation, geomagnetic activity, and other elements. Thus it is very important to consider the influences from both the configuration of geomagnetic field and the spinning of Earth for constructing the TEC empirical model. *Rawer* [1963, 1984] proposed a solution to above problem by adopting a coordinate system expressed by local time (LT) and the modified dip latitude (Modip) instead of simple geographic or geomagnetic coordinates. Recent studies have shown that the global features and variability within the ionosphere can be captured better by such a coordinate system [e.g., *Azpilicueta et al.*, 2006; *Zhang et al.*, 2009]. In the current study, we therefore adopted the coordinate (LT, Modip) for the data decomposition processes. The modified dip latitude is defined by equation (1) according to *Rawer* [1984].

$$Modip = \arctan\left(\frac{I}{\sqrt{\cos\varphi}}\right), \tag{1}$$

where I is the magnetic inclination angle, and φ is the geographic latitude.

[9] The processed global TEC data are decomposed as follows:

$$TEC(LT, Modip, UT, d) = \sum_{k=1}^{N} E_k(LT, Modip) \times P_k(UT, d), \tag{2}$$

where E_k(LT, Modip) are the EOF base functions that change with local time and modified dip latitude, which can represent the diurnal variation and spatial distribution of the original data. P_k(UT, d) are the associated coefficients that vary as a function of universal time and day, which can indicate the long-term temporal fluctuation of the original data. N represents the number of EOF 2D base functions. Table 1 lists the variances contributed by the first six EOF series. It can be seen that the contributions to the original data are 97.51%, 0.83%, 0.42%, and 0.28% for the first four EOF series, respectively, and 99.04% of the total variance in original data set can be accounted for in the combination of the first four EOF series, which manifests that the EOF decomposition converges quite quickly. So it is feasible to use only a few EOF base functions as well as the associated coefficients to represent most of the variation of the data set. Therefore, the number of modeling parameters is greatly reduced, while the accuracy of reconstruction remains considerably high.

[10] Figure 2 displays the contour plots of the first four orders of EOF base functions E_k in modified dip latitude and local time coordinates, while Figure 3 shows the distribution of the first four orders of coefficients P_k as a function of time and day. It is evident that the first-order base function E_1 shows mainly a diurnal variation, which closely resembles the latitude-local time distribution of the sample TEC shown in Figure 1. It is worth noting that E_1 contains a strong global average component that dominates the overall TEC variation since the first-order EOF series constitutes 97.51% of the total variance. Table 2 lists the correlation coefficients of the first four orders of EOF series with the solar and geomagnetic indices. The coefficient between the first order of EOF series and the $F_{10.7}$ index is as high as 0.886, while it is relatively weak for A_p, D_{st}, and *AE*. This phenomenon shows that the solar extremely ultraviolet (EUV) radiation is the major driver of the overall TEC variation [*Forbes et al.*, 2006], while geomagnetic activity plays a smaller but nonnegligible role.

[11] The second-order base function E_2 mainly displays a hemispherically asymmetric pattern, which can be attributed to the summer-to-winter annual variation induced by the uneven solar EUV illumination. This can be confirmed from Figure 3 with the second-order EOF coefficient P_2 which mainly contains an annual variation component. In addition, the second-order EOF series correlate weakly with $F_{10.7}$, A_p, and D_{st} indices, while a relatively stronger (although quite weak) correlation with *AE* is observed. This could possibly be caused by asymmetric auroral inputs due to one hemisphere being in darkness [*Newell et al.*, 1996]. This could drive asymmetric electron densities in the auroral zone and possibly neutral wind patterns that could cause hemispherically asymmetric electron densities. It can also be seen

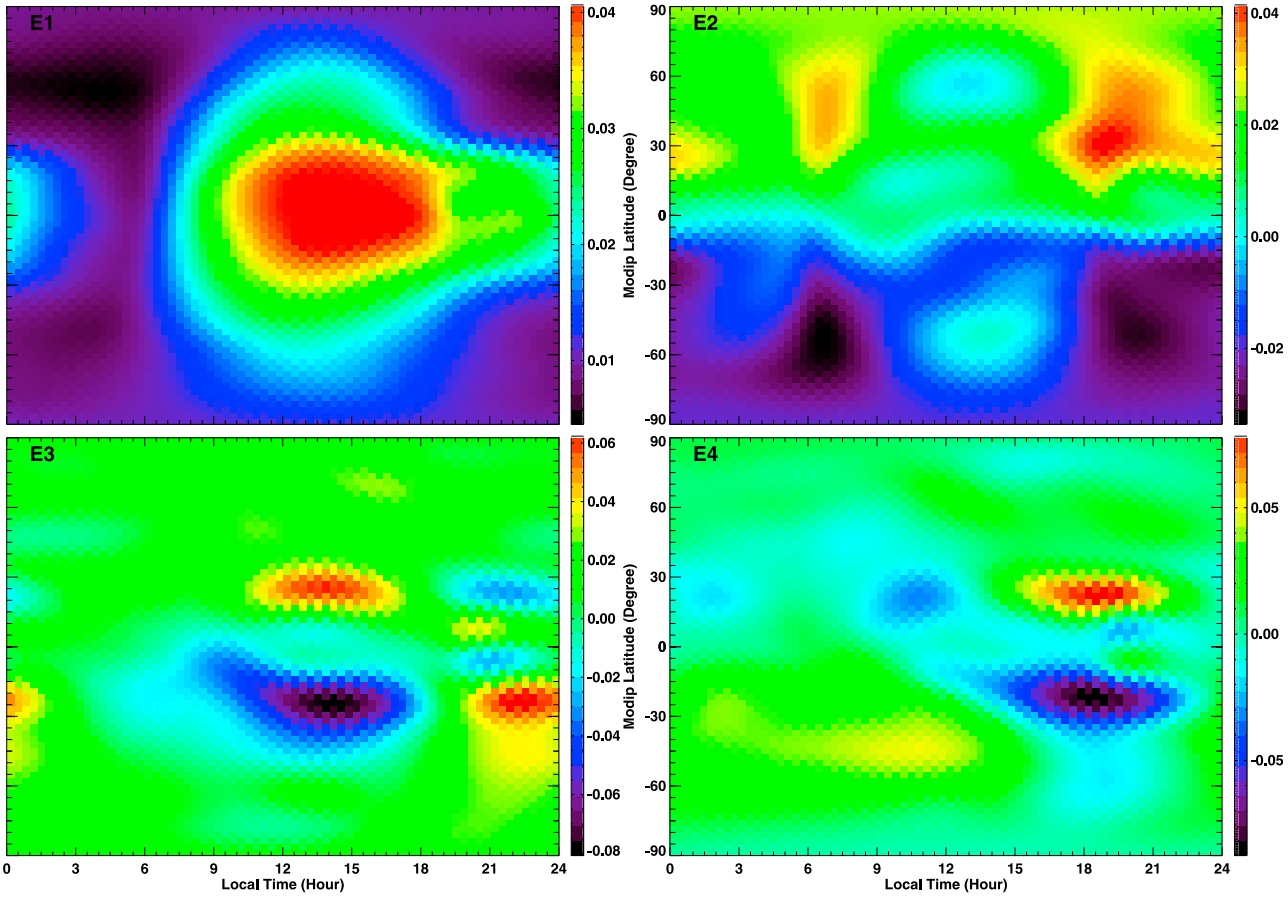

Figure 2. The distribution of the first four empirical orthogonal function (EOF) base functions through EOF decomposition of vertical TEC (VTEC) as a function of modified dip latitude and local time coordinate.

that there is a clear UT variation in P_2, which is due to the tilt of the Earth's magnetic field with respect to rotation axis.

[12] The most predominant feature of the third-order base function E_3 is the latitude distribution profile with positive/negative peaks located at about $\pm$ 20° modified dip latitude in each hemisphere and smaller variation components in between and outside, which is consistent with the well-known equatorial anomaly. A remarkable feature worth noticing is that the fourth-order base function E_4 also displays an evident "equatorial anomaly" phenomenon though it is more obvious in postsunset region. Considering the correlation coefficients, the fourth-order EOF series correlates weakly with $F_{10.7}$, A_p, and *AE* indices, while it exhibits highest correlation with D_{st} index. This explains that the phenomenon might be partly related to the low-latitude electrodynamics in storm time. During geomagnetically disturbed time, the upward (downward) E $\times$ B drift on the dayside (nightside) are weakened by the disturbance dynamo, which correspondingly results in weaker (stronger) equatorial anomaly on the dayside (nightside) [*Fejer et al.*, 1995; *Fuller-Rowell et al.*, 1997; *Maruyama et al.*, 2003; *Matsuo and Forbes*, 2010]. Therefore this phenomenon is most eminent in the prereversal enhancement region. Both P_3 and P_4 have very strong UT dependence, which can also be attributed to the distortion in the magnetic field.

[13] Another phenomenon worth noting is that there are some negative values of correlation coefficients for A_p, D_{st}, and *AE* indices in Table 2. This is because the solar geomagnetic driver and the response of TEC are not strictly simultaneous. In other words, there is time delay between the driving force and the response, which will certainly generate inverse correlation relationship. But in general, these negative values are very small, which seems lack of physical significance.

[14] Figure 4 displays the long-term variation of $F_{10.7}$, A_p, D_{st}, and *AE* indices during the time period 1999–2009. It can be seen from the comparison of Figures 3 and 4 that the first-order EOF coefficient P_1 indicates an obvious solar cycle variation pattern which depends strongly on solar activity represented by $F_{10.7}$ index. In order to better display the smaller-scale variation components, the wavelet power spectrum analysis method [*Grinsted et al.*, 2004] was used to further explore the first four orders of the EOF coefficients. Figure 5 shows the results. It can be seen from Figure 5 that P_1 mainly contains annual and semiannual variation components. The annual oscillation is the major variation component both in the second-order EOF coefficient P_2 and the third-order EOF coefficient P_3. The fourth-order EOF coefficient P_4 has both annual and semiannual variation components, with the magnitude of semiannual variation

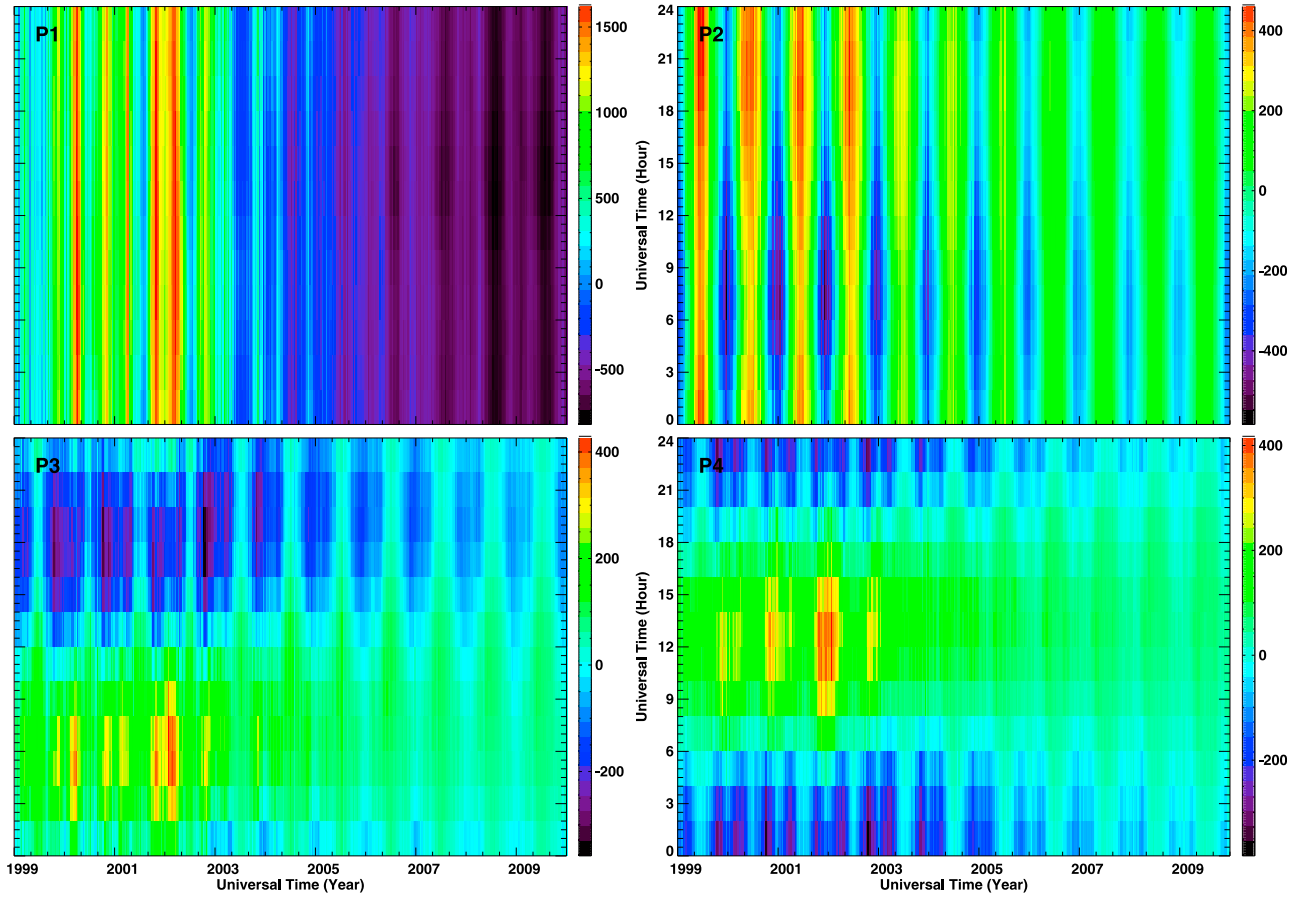

Figure 3. The distribution of the first four EOF coefficients through EOF decomposition of VTEC.

component becoming weaker than that of the annual variation with declining solar activity. In addition, P_3 also has a weak seasonal variation component (3–4 months).

[15] All of the four orders of EOF coefficients have a small amount of variations with periods around 1 month, but much more spread out. This could be due to the solar rotation variation components or the solar wind high-speed stream related to the distribution of the coronal holes on the Sun's chromosphere [*Lei et al.*, 2008; *Thayer et al.*, 2008], which indicates that the coefficients have certain dependence on solar activity.

[16] The aforementioned analysis shows that the EOF decomposition method is able to distribute the overall variance within the original data set into different components induced by corresponding drivers or mechanisms with respect to their relative contribution. For the model construction, here we need to implement a second EOF decomposition for the coefficients P_k(UT, d) as follows:

$$P_k(UT,d) = \sum_{n=1}^{M} B_{kn}(UT) \times A_{kn}(d), \tag{3}$$

where B_{kn}(UT) is the nth base function from EOF decomposition of P_k reflecting the variance with the universal time, while A_{kn}(d) is the associated nth coefficient representing the long-term variations. *M* is used to indicate the number of base functions for UT.

[17] Figure 6 displays the distribution of the first four orders of the base functions B_{kn} and the associated coefficients A_{kn} acquired from the second layer EOF decomposition. The base functions B_{kn} mainly contain diurnal variation components, while the coefficients A_{kn} represent the solar cycle, annual, and semiannual variation patterns and show a solar and geomagnetic activity dependence. Therefore, it is feasible to model the second layer coefficients A_{kn} using the following harmonic functions to represent the solar cycle, annual, and semiannual variations and to reflect the solar and geomagnetic activity dependence:

$$A_{kn}(d) = C_{kn1}(d) + C_{kn2}(d) + C_{kn3}(d) + \varepsilon \tag{4}$$

$$C_{kn1}(d) = D_{kn1} + E_{kn1}(d)F_{10.7p}(d) + F_{kn1}(d)A_p(d) + G_{kn1}D_{st}(d) + H_{kn1}(d)AE(d) \tag{5}$$

Table 2. Correlation Coefficients of the First Four Orders of the EOF Series With the Solar and Geomagnetic Indices

Correlation Coefficients	$F_{10.7}$ Index	A_p Index	D_{st} Index	*AE* Index
1st	0.886	0.212	−0.237	0.221
2nd	0.170	−0.061	0.065	0.282
3rd	0.084	−0.051	0.102	−0.038
4th	0.092	−0.053	0.247	−0.039

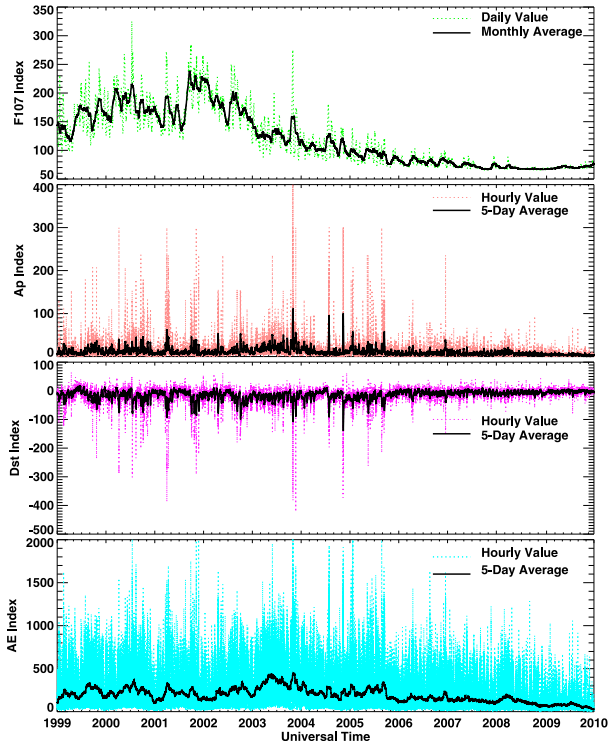

Figure 4. Long-term variation of $F_{10.7}$ index, A_p index, D_{st} index, and *AE* index during 1999–2009.

$$C_{kn2}(d) = (D_{kn2} + E_{kn2}(d)F_{10.7p}(d) + F_{kn2}(d)A_p(d) + G_{kn2}D_{st}(d) + H_{kn2}(d)AE(d))\cos\alpha + (I_{kn2} + J_{kn2}(d)F_{10.7p}(d) + K_{kn2}(d)A_p(d) + L_{kn2}D_{st}(d) + M_{kn2}(d)AE(d))\sin\alpha \quad (6)$$

$$C_{kn3}(d) = (D_{kn3} + E_{kn3}(d)F_{10.7p}(d) + F_{kn3}(d)A_p(d) + G_{kn3}D_{st}(d) + H_{kn3}(d)AE(d))\cos 2\alpha + (I_{kn3} + J_{kn3}(d)F_{10.7p}(d) + K_{kn3}(d)A_p(d) + L_{kn3}D_{st}(d) + M_{kn3}(d)AE(d))\sin 2\alpha \quad (7)$$

where C_{kn1}, C_{kn2}, and C_{kn3} correspond to the solar cycle, annual, and semiannual variation components in EOF coefficients A_{kn}, respectively. The C_{kn1}, C_{kn2}, and C_{kn3} are described as a combination of sinusoidal functions to represent different variation periods and linear functions of solar/geomagnetic indices to show their dependence on solar/geomagnetic activity. The factors D, E, F, G, H, I, J, K, L, and M can be calculated via least squares fitting method. $\alpha = 2\pi d/365.25$, ε is the residual error. $F_{10.7p} = (F_{10.7} + F_{10.7A})/2$, which was calculated based on the daily $F_{10.7}$ and its 81 day moving average $F_{10.7A}$. $F_{10.7p}$ has been used in solar irradiance empirical models as a solar EUV proxy [e.g., *Hinteregger et al.*, 1973; *Richards et al.*, 1994]. It was confirmed that the intensity of solar EUV flux can be well represented by $F_{10.7p}$ which has been considered to be a better solar proxy than normal $F_{10.7}$ for common use [*Liu et al.*, 2006, 2011]. The modeled coefficients A_{kn} can then be

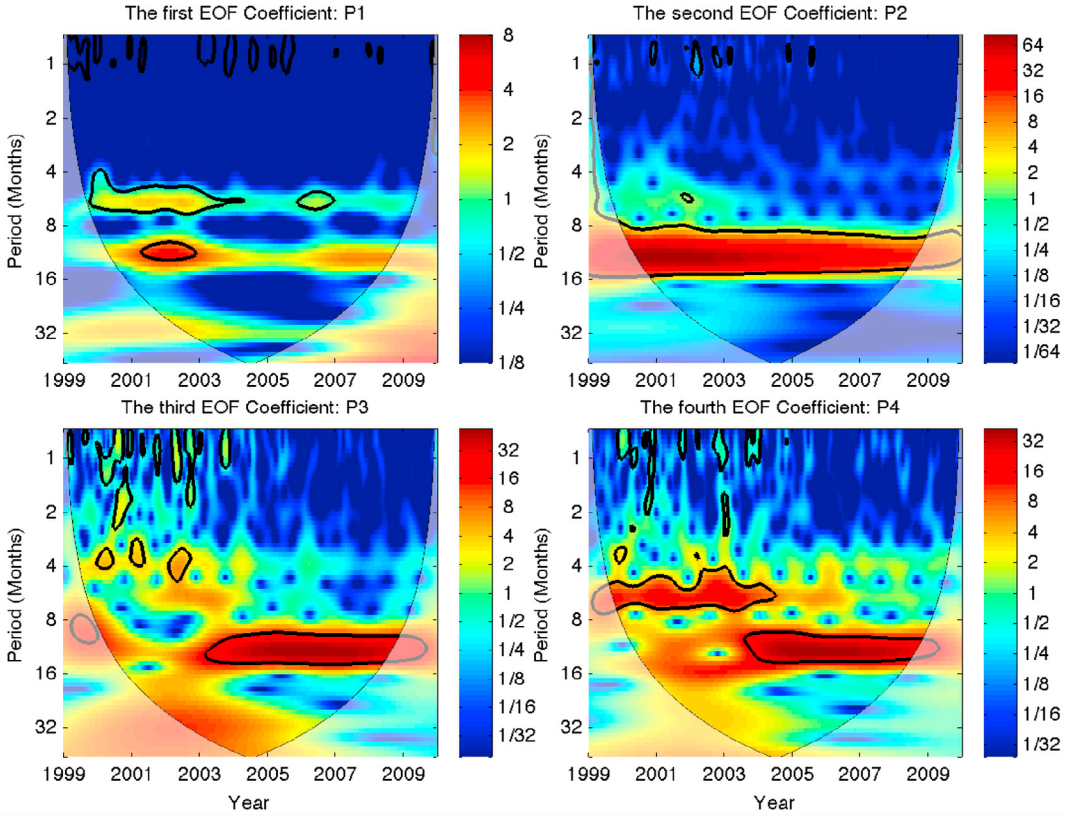

Figure 5. The wavelet power spectrum of the first four orders of EOF coefficients P_1–P_4. The thick black contour designates the 5% significance level against red noise. The cones of influence (COI) are shown as a lighter shade.

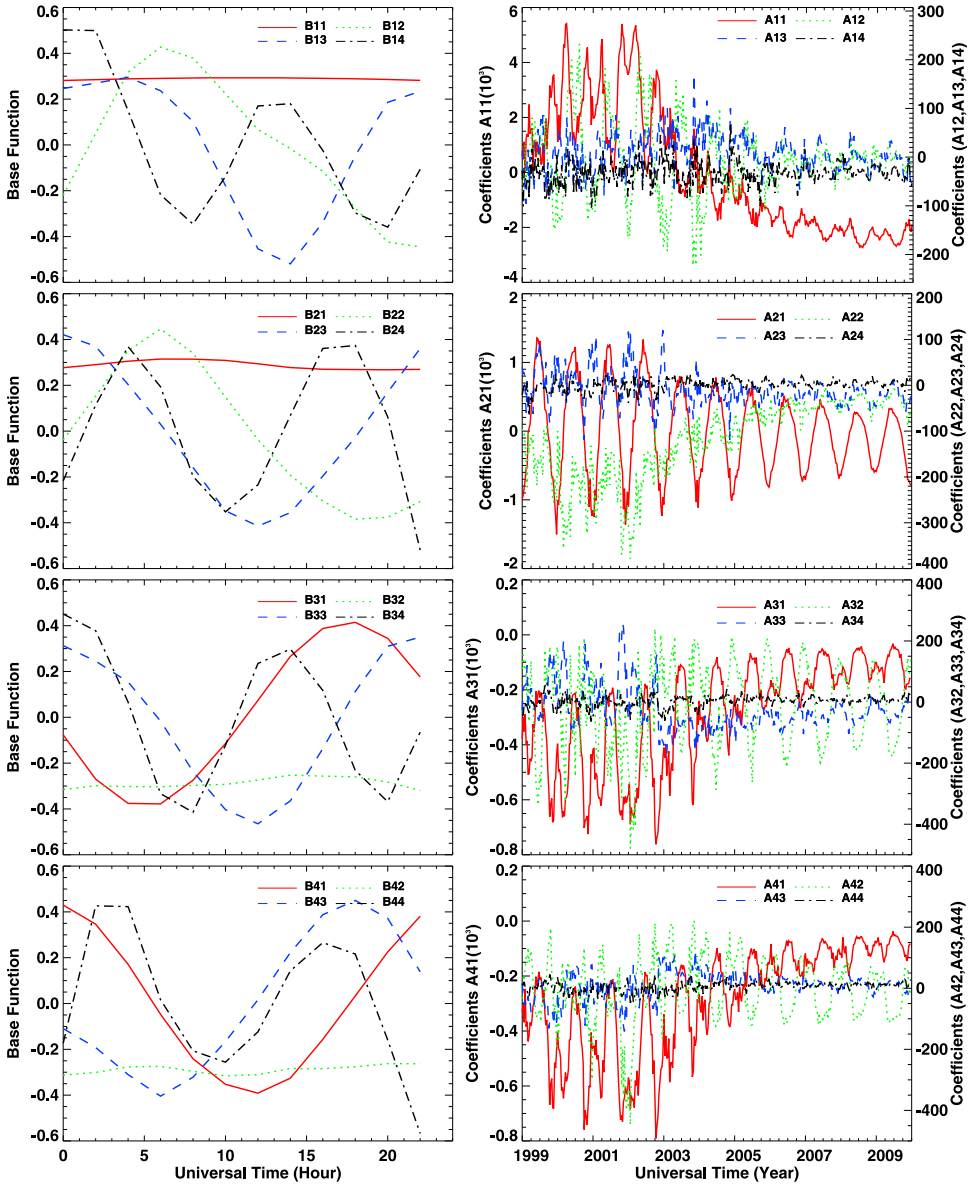

Figure 6. Distribution of (left) the base functions and (right) the associated coefficients acquired from the second layer EOF decomposition of TEC.

calculated utilizing inputs $F_{10.7p}$, A_p, D_{st}, and *AE* indices. With the modeled coefficients A_{kn} and the base functions B_{kn}, the modeled EOF coefficients P_k can be determined using equation (3). Finally, the modeled TEC value can be obtained with the modeled coefficients P_k and the base functions E_k using equation (2).

4. Model Validation

[18] In order to verify the validity of the global TEC model constructed by the double layered EOF method, here we will model the TEC value for each single year among 1999–2009, and then the TEC values calculated from the EOF model is used to make comparison with the original GIMs either globally or locally. Therefore the whole TEC data is modeled though we divide it into 11 parts based on natural year. One important thing worth noting is that the TEC data of each selected year for data-model comparison is excluded from the GIMs while building the EOF model. In other words, the data among the chosen time period is not included in the data set to produce the EOF coefficients. For example, the TEC model for 2002 used the GIMs data from the other 10 years (i.e., 1999 ∼ 2001 and 2003 ∼ 2009) while the data at 2002 is excluded. This makes the chosen data independent for model validation.

[19] After the above procedure, we first calculate the global mean TEC for the observed and modeled TEC by the following equation [*Afraimovich et al.*, 2008]:

$$TEC = \frac{1}{\sum_{i,j} S_{i,j}} \sum_{i,j} I_{i,j} \cdot S_{i,j}, \tag{8}$$

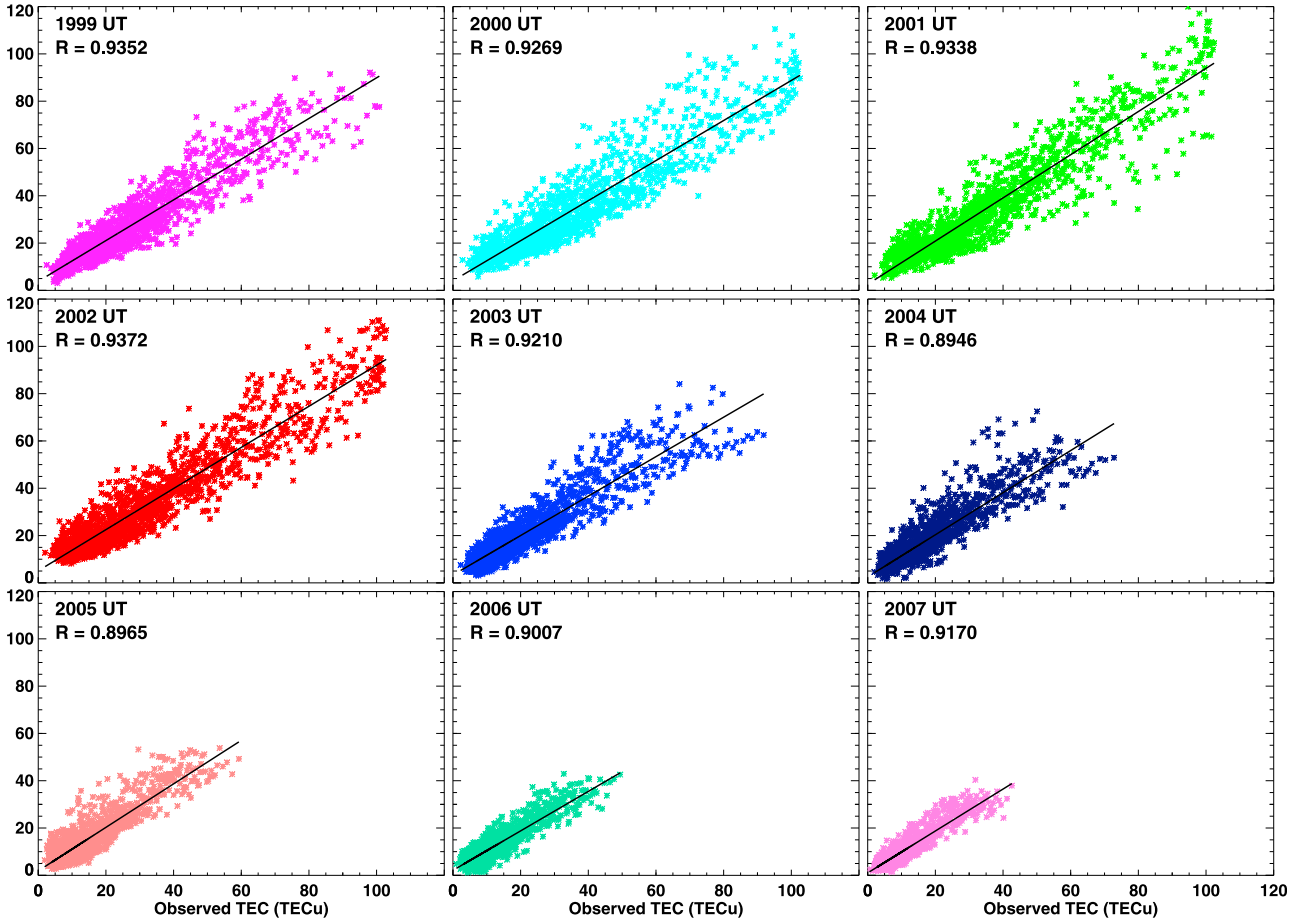

Figure 7. The comparison of scatterplots between modeled and observed values of TEC during the time period 1999–2007.

where i, j are the grid points along the latitude and longitude, respectively; $I_{i,j}$ is the TEC value in each grid cell, while $S_{i,j}$ is the associated area of the grid cell. Figure 7 displays the comparison of scatterplots between the modeled and observational values of TEC during the time period 1999–2007. It can be seen that the modeled global mean values correlate highly with the observational values of the global mean TEC, which indicates that the EOF model method can accurately represent the majority of the variations within the global mean observed within the original data set. In addition, the correlation coefficients are larger in high solar activity years than that in low solar activity years. This phenomenon has been observed in several studies for different ionospheric parameters using EOF model method [e.g., *Liu et al.*, 2008; *Zhang et al.*, 2009, 2010; *A et al.*, 2011]. It is more likely a typical feature of the EOF decomposition method, which might be induced by the larger cumulative percentage variances during high solar activity years than that in low solar activity years [*A et al.*, 2011].

[20] In order to better display the ability of the EOF model to reproduce the temporal-spatial feature of the TEC, Figures 8 and 9 show the global TEC maps in high solar activity year 2002 calculated from the JPL GIMs and modeled values, respectively. Both figures have four maps plotted corresponding to the vernal equinox, summer solstice, autumnal equinox, and winter solstice as a function of local time and geographic latitude. The modified dip latitude is also marked on the maps. Figures 10 and 11 show the similar TEC maps except for low solar activity year 2009. We can see that the feature of the TEC GIMs can be well reproduced by the EOF model, including both the large-scale and the smaller-scale features such as the sunset enhancement and equatorial anomaly. Yet there are some differences between the observed and model TEC which are mainly concentrated in the equatorial anomaly region. Further, it appears that the quality of the EOF model is better in the high solar activity year. This phenomenon is consistent with aforementioned studies.

[21] To further show the validity of the EOF model, Figures 12 and 13 display the comparison between the observed and modeled TEC at the same longitude (120°E) and eight different latitudes representing the high-latitude, midlatitude, and low-latitude regions for both Northern and Southern Hemispheres during high solar activity year 2002 and low solar activity year 2009, respectively. It can be seen that the value predicted by EOF model agrees quite well with the observed TEC.

[22] The deviation between the model and the observational data can be used to better investigate the accuracy of the EOF model at a single station. It is also necessary to

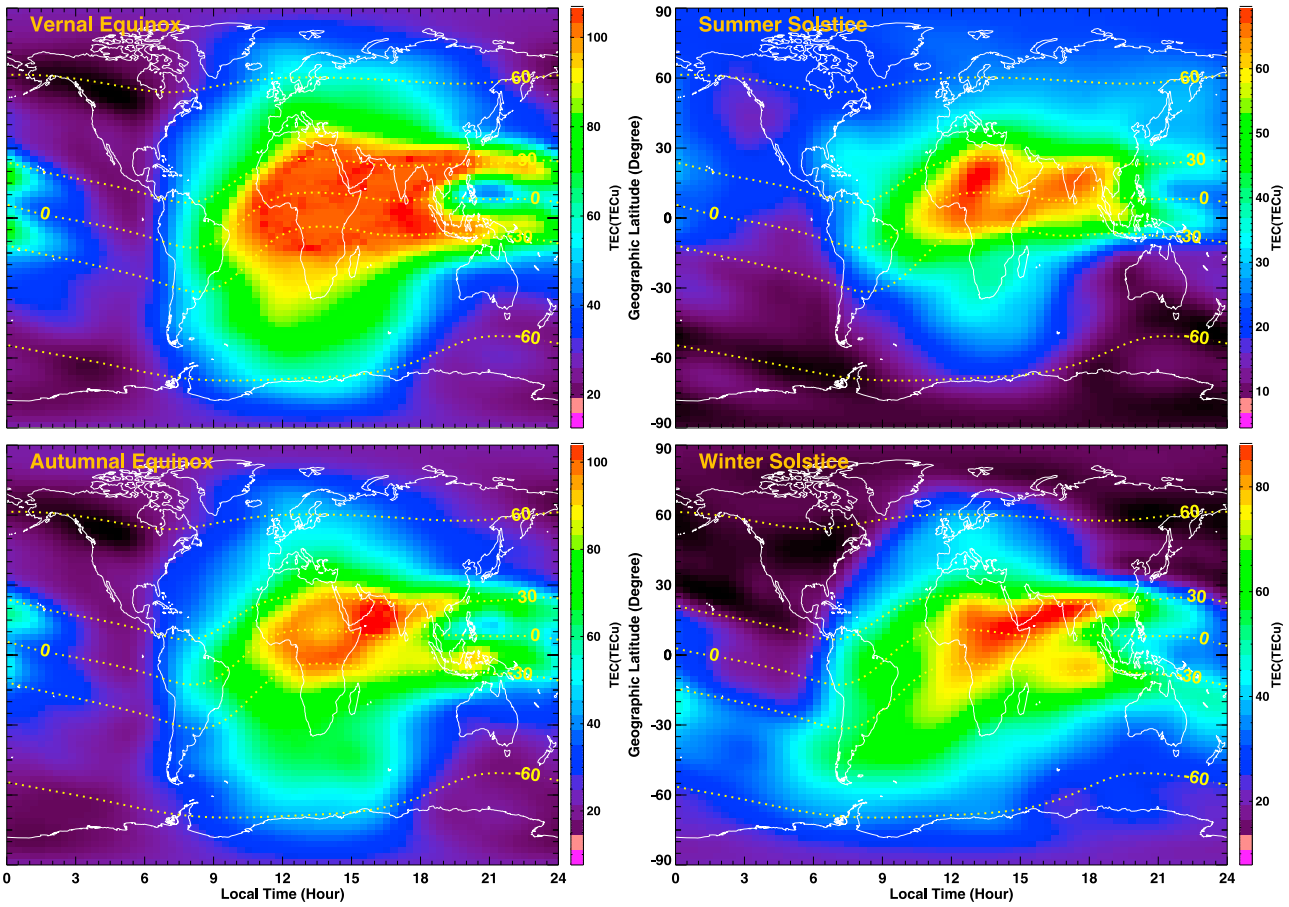

Figure 8. Global TEC maps calculated from Jet Propulsion Laboratory (JPL) global ionosphere maps (GIMs) at 12:00 UT for vernal equinox, summer solstice, autumnal equinox, and winter solstice during high solar activity year 2002. The modified dip latitude is also marked with white dots.

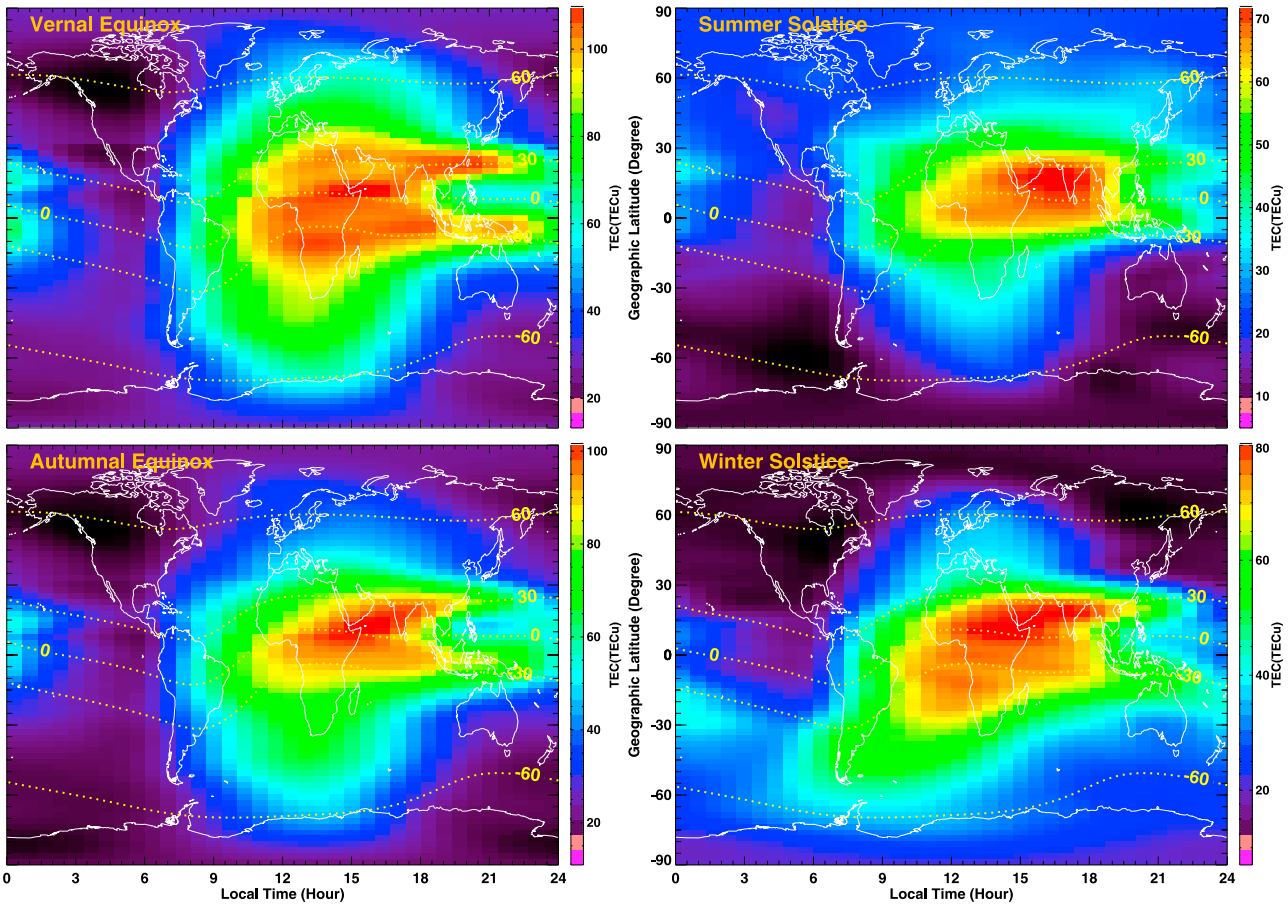

Figure 9. Global TEC maps calculated by EOF model at 12:00 UT for vernal equinox, summer solstice, autumnal equinox, and winter solstice during high solar activity year 2002. The modified dip latitude is also marked with white dots.

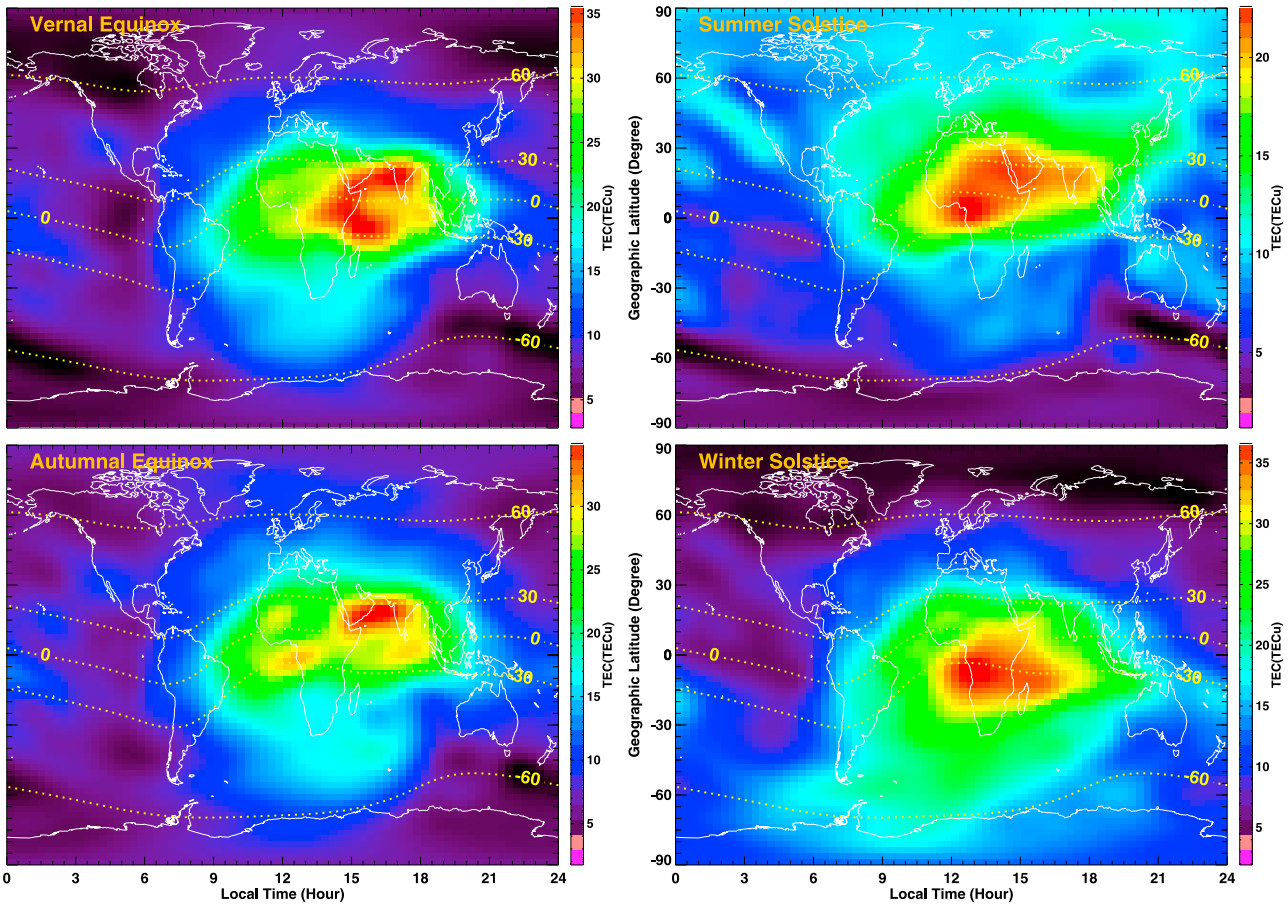

Figure 10. Global TEC maps calculated from JPL GIMs at 12:00 UT for vernal equinox, summer solstice, autumnal equinox, and winter solstice during low solar activity year 2009. The modified dip latitude is also marked with white dots.

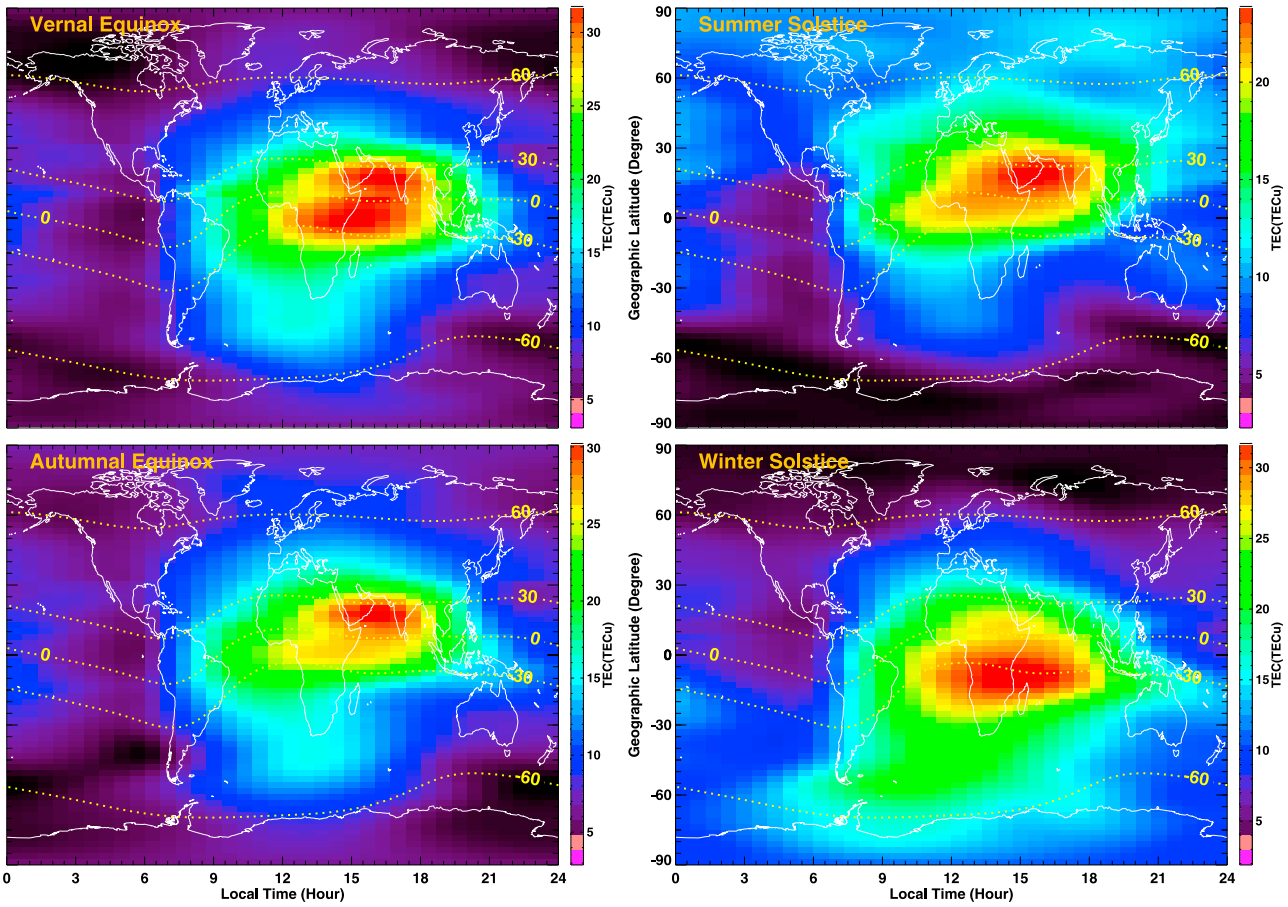

Figure 11. Global TEC maps calculated by EOF model at 12:00 UT for vernal equinox, summer solstice, autumnal equinox, and winter solstice during low solar activity year 2009. The modified dip latitude is also marked with white dots.

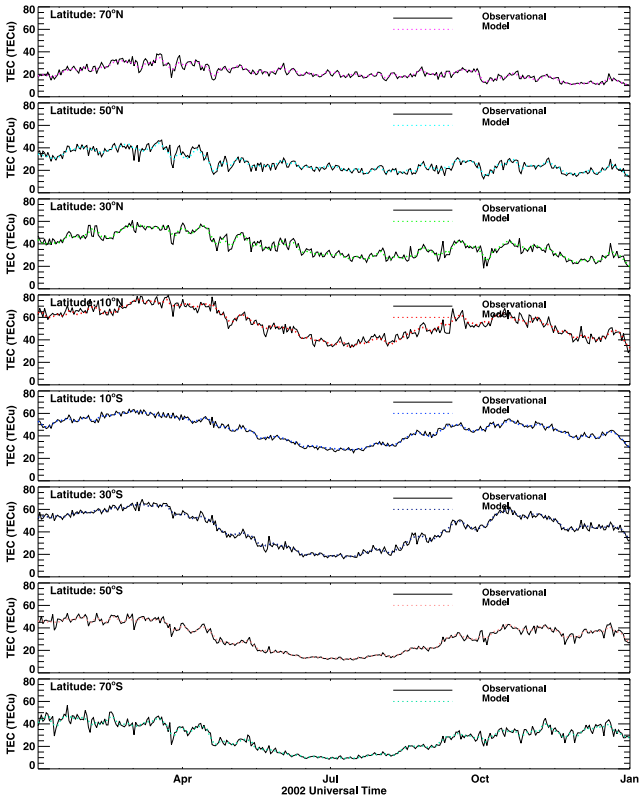

Figure 12. Comparison of observational and modeled TEC values at same longitude (120°E) and eight different latitudes for high solar activity year 2002.

compare the EOF model with other global ionospheric TEC models to better estimate there liability and validity of EOF model. Based on above consideration, the IRI model, one of the most widely used empirical models, is used to compare with the EOF model. Here a statistical analysis is implemented to calculate the relative difference (RD) and the normalized root mean square error (RMSE) between the observed and the modeled TEC values to make a quantitative validation:

$$RD = \frac{TEC_{mod} - TEC_{obs}}{TEC_{obs}} \times 100\%, \tag{9}$$

$$RMSE = \sqrt{\frac{1}{N_T}\sum_{i=1}^{N_T}\left(\frac{TEC_{mod} - TEC_{obs}}{TEC_{obs}}\right)^2} \times 100\%, \tag{10}$$

where RD is the average during a time period at a specific location and for each LT, and the N_T is the total number used for data-model comparison at all local times during the given time period.

[23] Figure 14 shows a sample plot of the diurnal variation of RD and RMSE between the TEC GIMs and modeled TEC values at Beijing (115.9°E, 39.6°N). The comparison is made for both high solar activity year 2002 and low solar activity year 2009 in spring (March, April, and May), summer (June, July, and August), autumn (September, October, and November), and winter (December, January, and February). It can be seen that the RD and RMSE calculated via EOF method is, in general, smaller than that acquired from IRI model. This demonstrates that the EOF model is able to better represent the majority of the variation in the original data set than that for IRI model. One thing worth carefully inspecting is that the RMSE of EOF in winter for high solar activity years are somewhat larger than the values in other seasons. This phenomenon, which is similar to the ionospheric winter anomaly, might be attributed to the large-scale interhemispheric circulation resulting into seasonal changes in the O/N_2 ratio during high solar activity. Hence the increase of ion production rate in winter hemisphere overwhelms the increase in wintertime lost rate. The anomaly enhancements of electron and ion density in winter will decelerate the velocity of the convergence of EOF decomposition, thereby further reduce the accumulated variance in the first four orders of the EOF series. Therefore the accuracy of model in winter is reduced.

[24] The validation of the EOF model during magnetic storms should also be considered. Figure 15 shows the comparison of JPL GIMs and EOF model on 30 October 2003 (i.e., Halloween storms). From the spatial perspective, the features shown in GIMs are reproduced not well by EOF model, especially in equatorial region. From the temporal perspective, the EOF model overunderestimate the TEC value during the main phase of the storm. Therefore it is quite challenging to capture the TEC dynamics during geomagnetic disturbed conditions. However, our consideration is

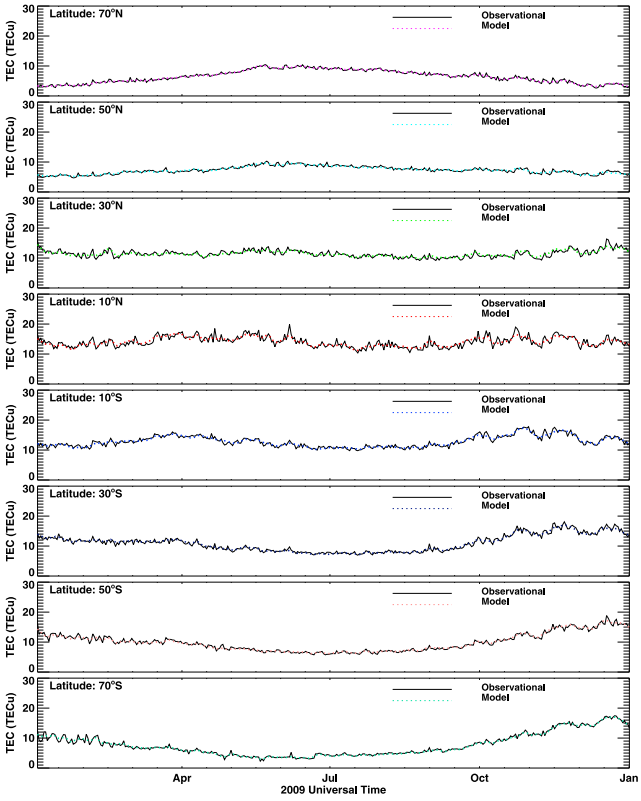

Figure 13. Comparison of observational and modeled TEC values at same longitude (120°E) and eight different latitudes for low solar activity year 2009.

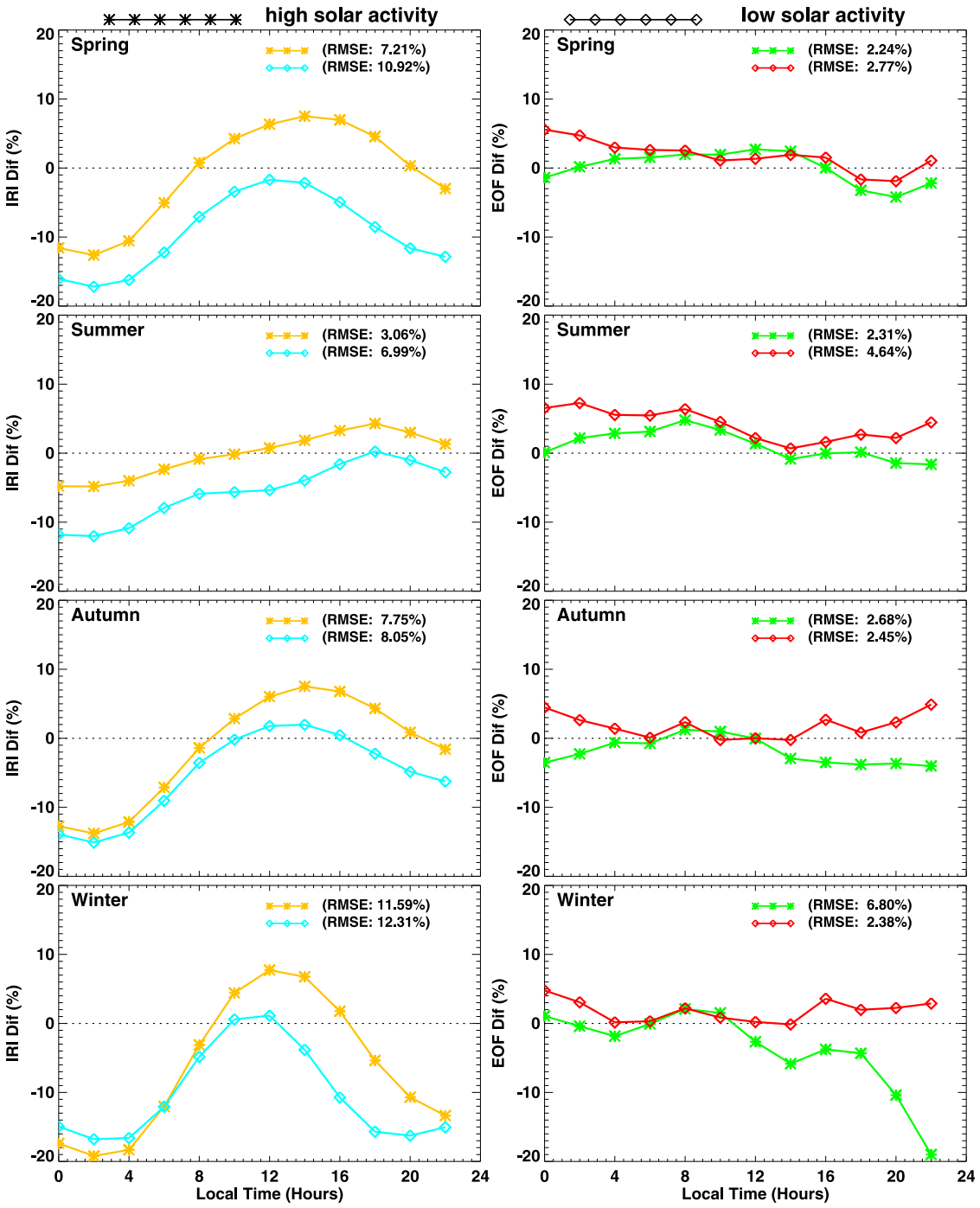

Figure 14. The diurnal variation of relative difference and normalized root mean square errors between the GIMs and modeled TEC data acquired from the International Reference Ionosphere and EOF models, respectively, at Beijing for both high and low solar activity years.

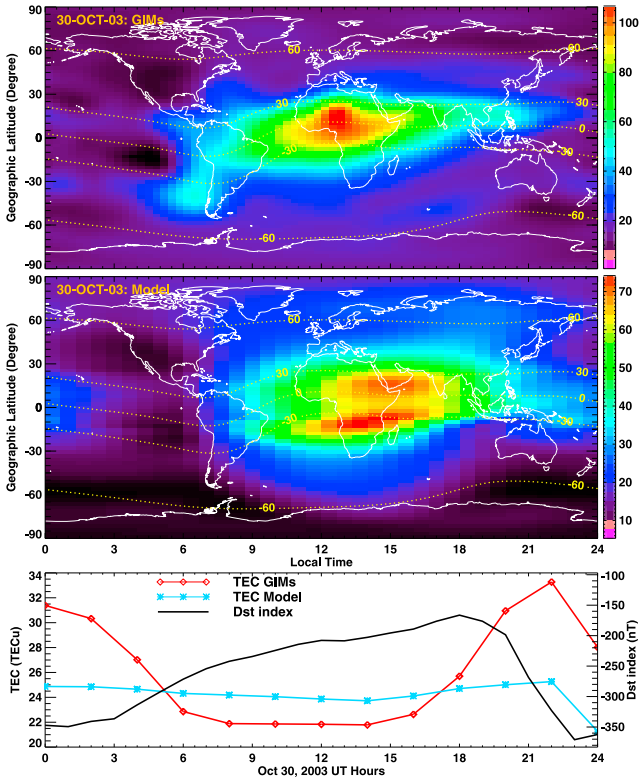

Figure 15. Comparison of TEC (top) GIMs and (middle) EOF model during magnetic storms at 12:00 UT on 30 October 2003. (bottom) Line plot of global mean TEC for GIMs and EOF model as well as the D_{st} index on 30 October 2003.

to construct an empirical model that can reflect the climatologically development of the TEC.

5. Summary and Conclusions

[25] In this study we present a global TEC model based on the EOF analysis method using the TEC GIMs during the time period 1999–2009 provided by JPL. The main findings and conclusions are:

[26] Firstly, it is much easier to capture the variability in the TEC when the data is converted into a coordinate system based on the magnetic dip latitude and local time. This removes significant amounts of variability that is simply due to the longitudinal dependence of the magnetic equator.

[27] Secondly, the first-order EOF base function E_1 represents a diurnal variation with a strong global average component, dominating most of the TEC variation. Solar EUV radiation and geomagnetic activity are the major drivers of E_1. The second-order EOF base function E_2 shows a hemispherically asymmetric pattern, indicating the summer-to-winter annual variation. This phenomenon may be attributed to the uneven solar EUV illumination. Both the third and fourth EOF base functions (E_3 and E_4) contain an evident equatorial anomaly phenomenon with positive/negative peaks located at about $\pm$ 20° modified dip latitude on each hemisphere and weak variation in between and outside.

[28] Thirdly, the first-order EOF coefficient P_1 contains an obvious solar cycle variation pattern as well as annual and semiannual variation components. The second-order EOF coefficient P_2 mainly includes annual fluctuation component. The third-order EOF coefficient P_3 contains a strong annual variation component and a weak seasonal variation pattern. The fourth-order EOF coefficient P_4 has both annual and semiannual oscillation components, while the magnitude of semiannual variation component becomes weaker than that of annual variation pattern with declining solar activity. Both P_3 and P_4 contain very strong diurnal variations which may be related to the magnetic field rotating around the Earth's rotation axis. All of the four EOF coefficients have somewhat variation components related to solar rotational variation or solar wind high-speed stream, which indicates their basic dependence on solar activity.

[29] Finally, the EOF decomposition method is able to separate the overall variance of the original data set into different variation components with respect to the associated drivers or mechanisms. The EOF decomposition converges quite quickly, thus it is possible to use only the a fourth-order EOF series to represent more than 99% of the total variance in the original data set. We constructed the TEC model using the trigonometric form of Fourier series described as a combination of sinusoidal functions with different periods to represent the solar cycle, annual, and semiannual variation components. Magnitudes are expressed with the linear functions of solar/geomagnetic indices to show their dependence on solar/geomagnetic activity. The data-model comparison implies that the model can reproduce quite well the observed TEC data set. The accuracy and quality of the model have been validated through the global-scale, regional, and single-station inspection as well as the statistical analysis. However, it is hard to use the climatologically developed EOF model to capture the dynamics of the TEC under geomagnetic disturbed conditions, which need to be studied using TEC data with much higher spatial-temporal resolution.

[30] **Acknowledgments.** This research was supported by the National Natural Science Foundation of China (40904036), National Important Basic Research Project of China (2011CB811405), and NASA grant NNG04GK18G. We gratefully acknowledge Aslak Grinsted for providing the Matlab software package for performing wavelet analysis. The $F_{10.7}$ and A_p indices are obtained from the NASA Goddard Space Flight Center Coordinated Data Analysis Web. The D_{st} and *AE* indices are obtained from the World Data Center for Geomagnetism, Kyoto, Japan.

[31] Robert Lysak thanks the reviewers for their assistance in evaluating this paper.

References

A, E., D.-H. Zhang, Z. Xiao, Y.-Q. Hao, A. J. Ridley, and M. Moldwin (2011), Modeling ionospheric *fo*F2 by using empirical orthogonal function analysis, *Ann. Geophys.*, *29*, 1501–1515, doi:10.5194/angeo-29-1501-2011.

Afraimovich, E. L., E. I. Astafyeva, A. V. Oinats, Y. V. Yasukevich, and I. V. Zhivetiev (2008), Global electron content: A new conception to track solar activity, *Ann. Geophys.*, *26*, 335–344, doi:10.5194/angeo-26-335-2008.

Azpilicueta, F., C. Brunini, and S. M. Radicella (2006), Global ionospheric maps from GPS observations using modip latitude, *Adv. Space Res.*, *38*, 2324–2331, doi:10.1016/j.asr.2005.07.069.

Bilitza, D. (Ed.) (1990), International Reference Ionosphere 1990, *Rep. 90–22*, Nat. Space Sci. Data Cent., Greenbelt, Md.

Bilitza, D. (2001), International Reference Ionosphere 2000, *Radio Sci.*, *36*, 261–275, doi:10.1029/2000RS002432.

Bilitza, D. (2002), Ionospheric models for radio propagation studies, in *The Review of Radio Science 1999–2002*, edited by W. R. Stone, pp. 625–679, IEEE Press, Piscataway, N. J.

Bouya, Z., M. Terkildsen, and D. Neudegg (2010), Regional GPS-based ionospheric TEC model over Australia using Spherical Cap Harmonic

Analysis, paper presented at 38th COSPAR Scientific Assembly, Comm. on Space Res., Bremen, Germany.
Bradley, P. (1999), Prediction and retrospective ionospheric modelling over Europe (PRIME), *Inf. Commun. Technol. COST Action Rep. 238*, Eur. Coop. in Sci. and Technol., Rutherford Appleton Lab., Didcot, U. K.
Daniell, R. E., L. D. Brown, D. N. Anderson, M. W. Fox, P. H. Doherty, D. T. Decker, J. J. Sojka, and R. W. Schunk (1995), Parameterized ionospheric model: A global ionospheric parameterization based on first principles models, *Radio Sci.*, *30*, 1499–1510, doi:10.1029/95RS01826.
Dow, J. M., R. E. Neilan, and C. Rizos (2009), The International GNSS Service in a changing landscape of Global Navigation Satellite Systems, *J. Geod.*, *83*, 191–198, doi:10.1007/s00190-008-0300-3.
Dvinskikh, N. I. (1988), Expansion of ionospheric characteristics fields in empirical orthogonal functions, *Adv. Space Res.*, *8*(4), 179–187, doi:10.1016/0273-1177(88)90238-4.
Fejer, B. G., E. R. de Paula, R. A. Heelis, and W. B. Hanson (1995), Global equatorial ionospheric vertical plasma drifts measured by the AE-E satellite, *J. Geophys. Res.*, *100*, 5769–5776, doi:10.1029/94JA03240.
Feltens, J. (2007), Development of a new three-dimensional mathematical ionosphere model at European Space Agency/European Space Operations Centre, *Space Weather*, *5*, S12002, doi:10.1029/2006SW000294.
Feltens, J., and S. Schaer (1998), IGS products for the ionosphere, IGS Position Paper, in *IGS 1998 Analysis Center Workshop: Proceedings*, edited by J. M. Dow, J. Kouba, and T. Springer, pp. 225–232, Eur. Space Oper. Cent., Darmstadt, Germany.
Forbes, J. M., S. E. Palo, and X. Zhang (2000), Variability of the ionosphere, *J. Atmos. Sol. Terr. Phys.*, *62*(8), 685–693, doi:10.1016/S1364-6826(00)00029-8.
Forbes, J. M., S. Bruinsma, and F. G. Lemoine (2006), Solar rotation effects on the thermospheres of Mars and Earth, *Science*, *312*, 1366–1368, doi:10.1126/science.1126389.
Fuller-Rowell, T. J., M. V. Codrescu, B. G. Fejer, W. Borer, F. Marcos, and D. N. Anderson (1997), Dynamics of the low-latitude thermosphere: Quiet and disturbed conditions, *J. Atmos. Sol. Terr. Phys.*, *59*, 1533–1540, doi:10.1016/S1364-6826(96)00154-X.
Fuller-Rowell, T., E. Araujo-Pradere, C. Minter, M. Codrescu, P. Spencer, D. Robertson, and A. R. Jacobson (2006), US-TEC: A new data assimilation product from the Space Environment Center characterizing the ionospheric total electron content using real-time GPS data, *Radio Sci.*, *41*, RS6003, doi:10.1029/2005RS003393.
Gao, Y., P. Heroux, and J. Kouba (1994), Estimation of GPS receiver and satellite L1/L2 signal delay biases using data from CACS, paper presented at the International Symposium on Kinematic Systems in Geodesy, Geomatics, and Navigation, Univ. of Calgary, Banff, Alberta, Canada.
Ge, S., et al. (2004), Comparison of TEC measurements from dual-frequency space geodetic techniques, *Eos Trans. AGU*, *85*(47), Fall Meet. Suppl., Abstract G53A-0118.
Grinsted, A., J. C. Moore, and S. Jevrejeva (2004), Application of the cross wavelet transform and wavelet coherence to geophysical time series, *Nonlinear Processes Geophys.*, *11*, 561–566.
Gulyaeva, T. L. (1999), Regional analytical model of ionospheric total electron content: Monthly mean and standard deviation, *Radio Sci.*, *34*, 1507–1512, doi:10.1029/1999RS900080.
Habarulema, J. B., L.-A. McKinnell, and B. D. L. Opperman (2010), TEC measurements and modelling over Southern Africa during magnetic storms; a comparative analysis, *J. Atmos. Sol. Terr. Phys.*, *72*, 509–520, doi:10.1016/j.jastp.2010.01.012.
Habarulema, J. B., L.-A. McKinnell, and B. D. L. Opperman (2011), Regional GPS TEC modeling; Attempted spatial and temporal extrapolation of TEC using neural networks, *J. Geophys. Res.*, *116*, A04314, doi:10.1029/2010JA016269.
Hanbaba, R. (1999), Improved quality of services in ionospheric telecommunication systems planning and operation, *Inf. Commun. Technol. COST Action Rep. 251*, Eur. Coop. in Sci. and Technol., Space Res. Cent., Warsaw.
Hernández-Pajares, M., J. M. Juan, and J. Sanz (1997), High-resolution TEC monitoring method using permanent ground GPS receivers, *Geophys. Res. Lett.*, *24*, 1643–1646, doi:10.1029/97GL01591.
Hernández-Pajares, M., J. M. Juan, and J. Sanz (1999), New approaches in global ionospheric determination using ground GPS data, *J. Atmos. Sol. Terr. Phys.*, *61*, 1237–1247, doi:10.1016/S1364-6826(99)00054-1.
Hernández-Pajares, M., J. M. Juan, J. Sanz, R. Orus, A. Garcia-Rigo, J. Feltens, A. Komjathy, S. C. Schaer, and A. Krankowski (2009), The IGS VTEC maps: A reliable source of ionospheric information since 1998, *J. Geod.*, *83*, 263–275, doi:10.1007/s00190-008-0266-1.
Hinteregger, H. E., D. E. Bedo, and J. E. Manson (1973), The EUV spectroheliometer on Atmosphere Explorer, *Radio Sci.*, *8*, 349–359, doi:10.1029/RS008i004p00349.
Ho, C. M., A. J. Mannucci, U. J. Lindqwister, X. Pi, and B. T. Tsurutani (1996), Global ionosphere perturbations monitored by the worldwide GPS network, *Geophys. Res. Lett.*, *23*, 3219–3222, doi:10.1029/96GL02763.
Iijima, B. A., I. L. Harris, C. M. Ho, U. J. Lindqwister, A. J. Mannucci, X. Pi, M. J. Reyes, L. C. Sparks, and B. D. Wilson (1999), Automated daily process for global ionospheric total electron content maps and satellite ocean altimeter ionospheric calibration based on Global Positioning System data, *J. Atmos. Sol. Terr. Phys.*, *61*, 1205–1218, doi:10.1016/S1364-6826(99)00067-X.
Jolliffe, I. T. (2002), *Principal Component Analysis*, 2nd ed., Springer, New York.
Lei, J., J. P. Thayer, J. M. Forbes, E. K. Sutton, and R. S. Nerem (2008), Rotating solar coronal holes and periodic modulation of the upper atmosphere, *Geophys. Res. Lett.*, *35*, L10109, doi:10.1029/2008GL033875.
Liu, C., M.-L. Zhang, W. Wan, L. Liu, and B. Ning (2008), Modeling M(3000)F2 based on empirical orthogonal function analysis method, *Radio Sci.*, *43*, RS1003, doi:10.1029/2007RS003694.
Liu, L., W. Wan, B. Ning, O. M. Pirog, and V. I. Kurkin (2006), Solar activity variations of the ionospheric peak electron density, *J. Geophys. Res.*, *111*, A08304, doi:10.1029/2006JA011598.
Liu, L., W. Wan, and H. Le (2011), Solar activity effects of the ionosphere: A brief review, *Chin. Sci. Bull.*, *56*, 1202–1211, doi:10.1007/s11434-010-4226-9.
Lorenz, E. N. (1956), Empirical orthogonal functions and statistical weather prediction, *Stat. Forecast Proj. Sci. Rep. 1*, Air Res. and Dev. Command, Andrews Air Force Base, Md.
Mannucci, A. J., B. D. Wilson, D. N. Yuan, C. H. Ho, U. J. Lindqwister, and T. F. Runge (1998), A global mapping technique for GPS-derived ionospheric total electron content measurements, *Radio Sci.*, *33*, 565–582, doi:10.1029/97RS02707.
Mao, T., W. Wan, X. Yue, L. Sun, B. Zhao, and J. Guo (2008), An empirical orthogonal function model of total electron content over China, *Radio Sci.*, *43*, RS2009, doi:10.1029/2007RS003629.
Marsh, D. R., S. C. Solomon, and A. E. Reynolds (2004), Empirical model of nitric oxide in the lower thermosphere, *J. Geophys. Res.*, *109*, A07301, doi:10.1029/2003JA010199.
Maruyama, N., S. Watanabe, and T. J. Fuller-Rowell (2003), Dynamic and energetic coupling in the equatorial ionosphere and thermosphere, *J. Geophys. Res.*, *108*(A11), 1396, doi:10.1029/2002JA009599.
Matsuo, T., and J. M. Forbes (2010), Principal modes of thermospheric density variability: Empirical orthogonal function analysis of CHAMP 2001–2008 data, *J. Geophys. Res.*, *115*, A07309, doi:10.1029/2009JA015109.
Matsuo, T., A. D. Richmond, and D. W. Nychka (2002), Modes of high-latitude electric field variability derived from DE-2 measurements: Empirical Orthogonal Function (EOF) analysis, *Geophys. Res. Lett.*, *29*(7), 1107, doi:10.1029/2001GL014077.
Matsuo, T., A. D. Richmond, and G. Lu (2005), Optimal interpolation analysis of high-latitude ionospheric electrodynamics using empirical orthogonal functions: Estimation of dominant modes of variability and temporal scales of large-scale electric fields, *J. Geophys. Res.*, *110*, A06301, doi:10.1029/2004JA010531.
Mendillo, M. (2006), Storms in the ionosphere: Patterns and processes for total electron content, *Rev. Geophys.*, *44*, RG4001, doi:10.1029/2005RG000193.
Newell, P. T., C.-I. Meng, and K. M. Lyons (1996), Suppression of discrete aurorae by sunlight, *Nature*, *381*, 766–767, doi:10.1038/381766a0.
Orús, R., M. Hernández-Pajares, J. M. Juan, and J. Sanz (2005), Improvement of global ionospheric VTEC maps by using Kriging interpolation technique, *J. Atmos. Sol. Terr. Phys.*, *67*, 1598–1609, doi:10.1016/j.jastp.2005.07.017.
Pearson, K. (1901), On lines and planes of closest fit to systems of points in space, *Philos. Mag.*, *2*, 559–572.
Ping, J., Y. Kono, K. Matsumoto, Y. Otsuka, A. Saito, C. Shum, K. Heki, and N. Kawano (2002), Regional ionosphere map over Japanese Islands, *Earth Planet. Space*, *54*, e13–e16.
Poulter, E. M., and J. K. Hargreaves (1981), A harmonic analysis of ATS-6 electron content observations at Lancaster, U.K. during 1975–6, *Ann. Geophy.*, *37*, 405–415.
Rawer, K. (1963), Propagation of decameter waves (HF-band), in *Meteorological and Astronomical Influences on Radio Wave Propagation*, edited by B. Landmark, pp. 221–250, Pergamon, Oxford, U. K.
Rawer, K. (Ed.) (1984), *Geophysics III, Encycl. Phys.*, vol. 7, pp. 389–391, Springer, New York.
Richards, P. C., J. A. Fennelly, and D. G. Torr (1994), EUVAC: A solar EUV flux model for aeronomic calculations, *J. Geophys. Res.*, *99*, 8981–8992, doi:10.1029/94JA00518.
Rishbeth, H., and M. Mendillo (2001), Patterns of F2-layer variability, *J. Atmos. Sol. Terr. Phys.*, *63*, 1661–1680, doi:10.1016/S1364-6826(01)00036-0.

Sayin, I., F. Arikan, and O. Arikan (2008), Regional TEC mapping with Random Field Priors and Kriging, *Radio Sci.*, *43*, RS5012, doi:10.1029/2007RS003786.

Schaer, S. (1999), *Mapping and Predicting the Earth's Ionosphere Using the Global Positioning System, Geod. Geophys. Arb. Schweiz.*, vol. 59, Inst. für Geod. und Photogramm., Zurich, Switzerland.

Singer, W., and N. I. Dvinskikh (1991), Comparison of empirical models of ionospheric characteristics developed by means of different mapping methods, *Adv. Space Res.*, *11*(10), 3–6, doi:10.1016/0273-1177(91)90311-7.

Stolle, C., S. Schlüter, S. Heise, C. Jacobi, N. Jakowski, S. Friedel, D. Kürschner, and H. Lühr (2005), GPS ionospheric imaging of the north polar ionosphere on 30 October 2003, *Adv. Space Res.*, *36*, 2201–2206, doi:10.1016/j.asr.2005.08.047.

Storch, H., and F. W. Zwiers (1999), *Statistical Analysis in Climate Research*, 484 pp., Cambridge Univ. Press, Cambridge, U. K.

Thayer, J. P., J. Lei, J. M. Forbes, E. K. Sutton, and R. S. Nerem (2008), Thermospheric density oscillations due to periodic solar wind high-speed streams, *J. Geophys. Res.*, *113*, A06307, doi:10.1029/2008JA013190.

Unnikrishnan, K., R. Balachandran Nair, and C. Venugopal (2002), Harmonic analysis and an empirical model for TEC over Palehua, *J. Atmos. Sol. Terr. Phys.*, *64*, 1833–1840, doi:10.1016/S1364-6826(02)00187-6.

Wan, W., L. Liu, and B. Ning (2008a), Modeling the global ionospheric TEC with statistical eigen mode analysis, paper presented at 37th COSPAR Scientific Assembly, Comm. on Space Res., Montreal, Que., Canada.

Wan, W., L. Liu, X. Pi, M.-L. Zhang, B. Ning, J. Xiong, and F. Ding (2008b), Wavenumber-4 patterns of the total electron content over the low latitude ionosphere, *Geophys. Res. Lett.*, *35*, L12104, doi:10.1029/2008GL033755.

Wan, W., F. Ding, M. Zhang, L. Liu, and B. Ning (2012), Modeling the global ionospheric total electron content with empirical orthogonal function analysis, *Sci. China, Ser. E*, in press.

Wilson, B. D., A. J. Mannucci, and C. D. Edwards (1995), Subdaily Northern Hemisphere ionospheric maps using an extensive network of GPS receivers, *Radio Sci.*, *30*, 639–648, doi:10.1029/94RS03186.

Xu, W., and Y. Kamide (2004), Decomposition of daily geomagnetic variations by using method of natural orthogonal component, *J. Geophys. Res.*, *109*, A05218, doi:10.1029/2003JA010216.

Zapfe, B., M. Materassi, C. Mitchell, and P. Spalla (2006), Imaging of the equatorial ionospheric anomaly over South America–A simulation study of total electron content, *J. Atmos. Sol. Terr. Phys.*, *68*, 1819–1833, doi:10.1016/j.jastp.2006.05.025.

Zhang, D. H., and Z. Xiao (2003), Study of the ionospheric total electron content response to the great flare on 15 April 2001 using the International GPS Service network for the whole sunlit hemisphere, *J. Geophys. Res.*, *108*(A8), 1330, doi:10.1029/2002JA009822.

Zhang, M., C. Liu, W. Wan, L. Liu, and B. Ning (2009), A global model of the ionospheric F2 peak height based on EOF analysis, *Ann. Geophys.*, *27*, 3203–3212, doi:10.5194/angeo-27-3203-2009.

Zhang, M.-L., C. Liu, W. Wan, L. Liu, and B. Ning (2010), Evaluation of global modeling of M(3000)F2 and hmF2 based on alternative empirical orthogonal function expansions, *Adv. Space Res.*, *46*, 1024–1031, doi:10.1016/j.asr.2010.06.004.

Zhao, B., W. Wan, L. Liu, X. Yue, and S. Venkatraman (2005), Statistical characteristics of the total ion density in the topside ionosphere during the period 1996–2004 using empirical orthogonal function (EOF) analysis, *Ann. Geophys.*, *23*, 3615–3631, doi:10.5194/angeo-23-3615-2005.

E. A and A. J. Ridley, Department of Atmospheric, Oceanic, and Space Sciences, University of Michigan, 2455 Hayward St., Ann Arbor, MI 48109, USA. (aercha@umich.edu; ridley@umich.edu)

Y. Hao, Z. Xiao, and D. Zhang, Institute of Space Physics and Applied Technology, Peking University, Beijing 100871, China. (zhangdh@pku.edu.cn)